

N. G. Stefanis

# Pion-photon transition form factor.

Living on the QCD frontier

Received: 31-08-2011 / Accepted: 12-09-2011

**Abstract** An analysis of all available data (CELLO, CLEO, *BABAR*) in the range  $[1 \div 40]$   $\text{GeV}^2$  for the pion-photon transition form factor in terms of light-cone sum rules with next-to-leading-order accuracy is discussed, including twist-four contributions and next-to-next-to-leading order and twist-six corrections—the latter two via uncertainties. The antithetic trend between the *BABAR* data for the  $\gamma^*\gamma\pi^0$  and those for the  $\gamma^*\gamma\eta(\eta')$  transition is pointed out, emphasizing the underlying antagonistic mechanisms: endpoint enhancement for the first and endpoint-suppression for the second—each associated with pseudoscalar meson distribution amplitudes with distinct endpoint characteristics.

**Keywords** Transition form factors · pion distribution amplitude · light-cone sum rules

## 1 Introduction

This is a report about the pion-photon transition form factor—an observable that is considered to be the prime example of an exclusive process in QCD because in leading order (LO) the partonic interactions are purely electrodynamic, with the strong interactions being factorized out into the pion distribution amplitude (DA). While the accuracy of the CELLO data [1] was not sufficient to provide a proof-of-concept of the QCD framework, the appearance of the CLEO data [2] established the validity of the collinear factorization of this process [3]. This situation changed dramatically in the year 2009 when the *BABAR* Collaboration published new data [4] with very small error bars at intermediate momentum transfers reaching values just below  $40 \text{ GeV}^2$ —unreachable in the past—with still tolerable errors. These data for the scaled form factor  $Q^2 F^{\gamma^*\gamma\pi^0}(Q^2)$  exhibit two distinctive features: (i) The earlier data taken by CLEO at the *same* momentum-transfer values were confirmed, but with a higher accuracy. (ii) Unexpectedly, the data starting above  $9 \text{ GeV}^2$  and extending up to about  $40 \text{ GeV}^2$  do not scale with  $Q^2$ . Instead, they show a clear general tendency to rapidly grow with  $Q^2$ , with the exception of two single data points at about  $14 \text{ GeV}^2$  and  $27 \text{ GeV}^2$  that lie just below the asymptotic prediction of perturbative QCD [3]:  $\lim_{Q^2 \rightarrow \infty} Q^2 F^{\gamma^*\gamma\pi^0} \rightarrow \sqrt{2} f_\pi$ . Understanding the underlying enhancement mechanism(s), responsible for this behavior, is of significant importance because an increasing form factor challenges the basic concepts of QCD, like collinear factorization. The recent analysis in Ref. [5], reported here, builds on light-cone sum rules (LCSR)s by taking into account various contributions from perturbative and nonperturbative QCD and by utilizing in the analysis data sets from different experiments [1; 2; 4] for momentum-transfer values ranging from 1 to  $40 \text{ GeV}^2$ . Emphasis is given

---

Presented at LIGHTCONE 2011, 23 - 27 May, 2011, Dallas, USA

N. G. Stefanis  
Institut für Theoretische Physik II, Ruhr-Universität Bochum, D-44780 Bochum, Germany  
Tel.: +49-234-3223724  
Fax: +49-234-3214248  
E-mail: stefanis@tp2.ruhr-uni-bochum.de

to the statistical features and the way they depend on the various theoretical parameters. The main goal is the confrontation of theoretical predictions, obtained with the help of light-cone sum rules (LCSR)s, with all available experimental data for the pion-photon transition form factor. In addition, the results are compared with the *BABAR* data [6] for the  $\eta$ - and  $\eta'$ -photon transition form factors making use of the description of the  $\eta - \eta'$  mixing in the quark flavor basis [7] that involves the state  $|n\rangle = (|\bar{u}u\rangle + |\bar{d}d\rangle)/\sqrt{2}$ . This makes it possible to link the  $\gamma^*\gamma \rightarrow |n\rangle$  transition form factor, multiplied by  $3/5$ , to the form factor  $\gamma^*\gamma \rightarrow \pi^0$ , where the prefactor arises from the quark charges.

## 2 Computational Method

The method of light-cone sum rules, developed in [8] for the pion-photon transition form factor, but not only [9], has been refined by years of experience in many analyses [10; 11; 12; 13; 5]. It contains a set of rules that encode a computational model and as any model it encodes *implicit* predictions that turn *explicit* under some justified assumptions about its inherent (and auxiliary) parameters. The subtlety is how to adjust these parameters in such a way as to achieve the best possible accuracy of the obtained predictions with respect to the experimental data while avoiding sensitivity on particular values.

The modulus operandi of the LCSRs for the pion-photon transition form factor is expressed by [8]

$$Q^2 F^{\gamma^* \gamma \pi}(Q^2) = \frac{\sqrt{2}}{3} f_\pi \left[ \frac{Q^2}{m_\rho^2} \int_{x_0}^1 \exp\left(\frac{m_\rho^2 - Q^2 \bar{x}/x}{M^2}\right) \bar{\rho}(Q^2, x) \frac{dx}{x} + \int_0^{x_0} \bar{\rho}(Q^2, x) \frac{dx}{\bar{x}} \right], \quad (1)$$

where the abbreviations  $s = \bar{x}Q^2/x$  and  $x_0 = Q^2/(Q^2 + s_0)$  have been used, and with the spectral density  $\bar{\rho}(Q^2, x) = (Q^2 + s)\rho^{\text{PT}}(Q^2, s)$  taken with next-to-leading-order (NLO) accuracy. The hadronic threshold in the vector-meson channel has the value  $s_0 = 1.5 \text{ GeV}^2$ ,  $M$  is the Borel parameter, and  $m_\rho = 0.77 \text{ GeV}$  denotes the physical mass of the  $\rho$  meson. The first term in (1) stems from the hadronic content of a quasireal photon at low  $s \leq s_0$ , while the second one resembles its pointlike behavior at higher  $s > s_0$ . The main advantage of employing LCSRs is that one starts with the situation where both photon virtualities are sufficiently large, so that perturbation theory is safely applicable, and approaches the asymmetric kinematics with  $Q^2$  fixed and large and  $q^2 \rightarrow 0$  via a dispersion relation:

$$F^{\gamma^* \gamma^* \pi}(Q^2, q^2) = \int_0^\infty ds \frac{\rho(Q^2, s)}{s + q^2}, \quad (2)$$

where the physical spectral density  $\rho(Q^2, s)$  approaches at large  $s$  the perturbative one:  $\rho^{\text{PT}}(Q^2, s) = \frac{1}{\pi} \text{Im} F^{\gamma^* \gamma^* \pi}(Q^2, -s - i\varepsilon)$ . The form factor  $F^{\gamma^* \gamma^* \pi}(Q^2, q^2)$  can be calculated via perturbative QCD having recourse to collinear factorization, meaning that it can be written in the convolution form [3; 14]

$$F^{\gamma^* \gamma^* \pi}(Q^2, q^2) = \frac{\sqrt{2}}{3} f_\pi \int_0^1 dx T(Q^2, q^2, \mu_F^2, x) \varphi_\pi^{(2)}(x, \mu_F^2) + O(\delta^2/Q^4), \quad (3)$$

where the pion decay constant is  $f_\pi = 132 \text{ MeV}$  and  $\delta^2$  is the twist-four coupling. All nonperturbative information of the bound state is encapsulated in the coefficients  $a_n$  that are incalculable within perturbation theory and have to be modeled, or be computed on the lattice, e.g., [15; 16], via the moments  $\langle \xi^N \rangle_\pi \equiv \int_0^1 dx (2x - 1)^N \varphi_\pi^{(2)}(x, \mu^2)$  with the normalization condition  $\int_0^1 dx \varphi_\pi^{(2)}(x, \mu^2) = 1$ . The leading twist-two pion DA fulfills an evolution equation [3; 14] and can be expressed in terms of the Gegenbauer polynomials  $C_n^{3/2}(2x - 1)$  to read

$$\varphi^{(2)}(x, \mu^2) = \varphi^{\text{as}}(x) + \sum_{n=2,4,\dots} a_n(\mu^2) \psi_n(x), \quad (4)$$

where  $\psi_n(x) = 6x(1-x)C_n^{3/2}(2x-1)$  and  $\varphi^{\text{as}}(x) = \psi_0(x) = 6x(1-x)$  is the asymptotic pion DA [3; 14].

The cornerstones of the analysis in [5], on which this report is based, are:

- NLO radiative corrections: They are taken into account in the spectral density [12], after correcting the error pointed out in [13], and using  $\mu_{\text{fact}}^2 = \mu_{\text{ren}}^2 = Q^2$  to avoid (large) logarithms of these scales. They are negative leading to suppression of the transition form factor.

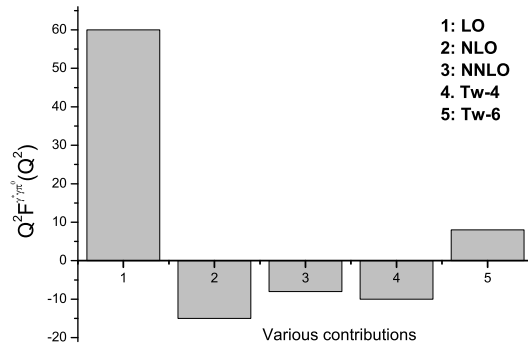


**Fig. 1** (color online) Illustration of the various contributions to the pion-photon transition form factor.

- Twist-four contributions: They are included via the coupling  $\delta^2(\mu^2) \in [0.15 \div 0.23] \text{ GeV}^2$  and performing one-loop evolution assuming the asymptotic form for the twist-four pion DA:  $\varphi_{\pi}^{(4)}(x, \mu^2) = (80/3)\delta^2(\mu^2) x^2(1-x)^2$ . [Nonasymptotic forms were found before to be of minor importance.] These contributions are also negative and yield suppression.
- Evolution of the coefficients  $a_n$ : They are included at the NLO level of accuracy, using the QCD scale parameters  $\Lambda_{\text{QCD}}^{(N_f=3)} = 370 \text{ MeV}$  and  $\Lambda_{\text{QCD}}^{(N_f=4)} = 304 \text{ MeV}$ , and provide suppression.
- NNLO $_{\beta_0}$  (for next-to-next-to-leading) radiative corrections [17] and twist-six contributions [13]: They are taken into account implicitly in terms of theoretical uncertainties. This is justified because for the average value of  $M^2(Q^2) \sim 0.75 \text{ GeV}^2$ , used in our analysis [5], the net result of adding these (not large) terms is small, decreasing with  $Q^2$  from  $+0.005$  at  $Q^2 = 1 \text{ GeV}^2$ —where the positive twist-six term prevails—down to  $-0.003$  at  $Q^2 = 40 \text{ GeV}^2$ —where the negative NNLO correction becomes stronger. Note that for  $M^2 = 1.5 \text{ GeV}^2$  [13], the twist-six term becomes negligible, while NNLO $_{\beta_0}$  still provides suppression.
- Inclusion of resonances: A finite-width Breit-Wigner form is adopted in the spectral density in order to resolve the  $\rho$  and  $\omega$  resonances [8; 12]. This entails a small enhancement of the transition form factor as compared to the  $\delta$ -function ansatz.

Figure 1 illustrates the approximate composition of the pion-photon transition form factor.

### 3 Theoretical Predictions and Comparison with Data

We now have all the elements for the data analysis. In order to get the most output from the data for the pion-photon transition form factor [1; 2; 4] and achieve the best insight about the particular role and relative strength of the first three Gegenbauer coefficients  $a_2, a_4, a_6$ , we divide the data into two sets: (a)  $[1 \div 9] \text{ GeV}^2$ —termed ‘CLEO regime’ and (b)  $[1 \div 40] \text{ GeV}^2$ —‘entire range’. The results of the statistical 3-D analysis of these data sets are displayed in Fig. 2—upper part—in the left and right panel, respectively, using the central value  $\delta^2 = 0.19 \text{ GeV}^2$  of the twist-four coupling. Both panels show the corresponding  $1\sigma$  ellipsoids which are characterized by their principal axes and ellipses. The projection of the  $1\sigma$  ellipsoid on the plane  $(a_2, a_4)$  is represented, in both panels, by the larger ellipse enclosed by a solid line in red color. The smaller enclosed ellipse in the left panel denotes the cross section of the ellipsoid with the  $(a_2, a_4)$  plane, whereas the shaded (green) rectangle shows the region in the  $(a_2, a_4)$  plane allowed by nonlocal QCD sum rules [18], with the point in the center (marked by  $\mathbf{x}$ ) denoting the Bakulev-Mikhailov-Stefanis (BMS) pion DA [18]. The profile of this DA exhibits a double-humped structure with suppressed endpoints  $x = 0, 1$  due to the use of nonlocal condensates [18]—see also [19] for a discussion of the endpoint region of the pion DA. All results are shown at the scale  $\mu_{\text{SY}}^2 = (2.4 \text{ GeV})^2$  after NLO evolution. Performing the analysis with the second data set (upper right panel), entails a sizeable coefficient  $a_6$ , so that the  $1\sigma$  ellipsoid is lifted off the plane  $(a_2, a_4)$ , while its projection remains almost the same as in the left panel. Remarkably, it still overlaps with the shaded rectangle containing the BMS model and the constraints from nonlocal QCD sum rules [18].

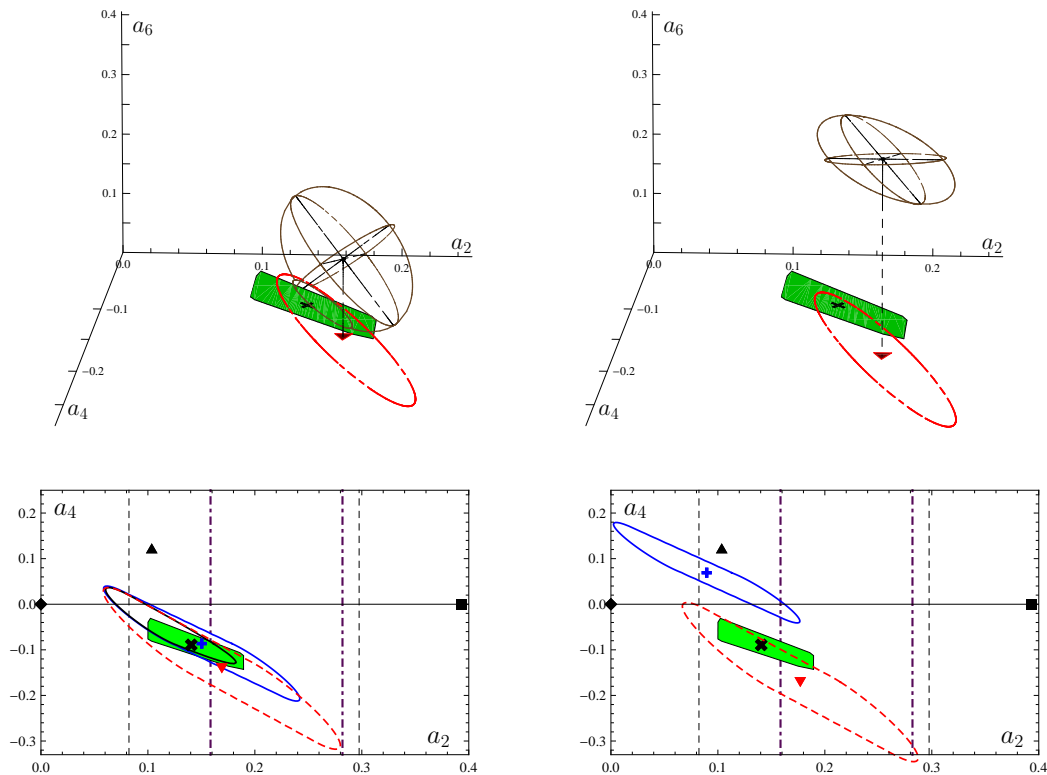


**Fig. 2** (color online). Upper panels show 3-D graphics of  $1\sigma$  error ellipsoids in Gegenbauer space  $(a_2, a_4, a_6)$ . Lower panels show  $1\sigma$  error ellipsoids in the  $(a_2, a_4)$  space resulting from unifying  $1\sigma$  ellipses pertaining to the values of the twist-four coupling  $\delta^2 = 0.15, 0.19, 0.23 \text{ GeV}^2$ . Left panels refer to the analysis of all data [1; 2; 4] in the range  $[1 \div 9] \text{ GeV}^2$ , whereas the right panels give the analogous results for the region  $[1 \div 40] \text{ GeV}^2$ .

Attempting to understand more quantitatively how the twist-four contribution affects our results, we concentrate on the  $(a_2, a_4)$  plane and present our findings in the lower part of Fig. 2 in terms of  $1\sigma$  ellipses. These are calculated by varying the  $\delta^2$  coupling from 0.15 to 0.19 to 0.23  $\text{GeV}^2$  and then merging the obtained  $1\sigma$  error ellipses together to form the distorted ellipses shown in this graphics. Left panel (‘CLEO regime’): The largest ellipse—dashed (red) line—results from combining the projections on the plane  $(a_2, a_4)$  of the 3-D data analysis discussed before. The smaller ellipse (solid blue line) shows the outcome of a 2-D analysis by means of  $a_2$  and  $a_4$ . Its middle point with the coordinates  $(0.15, -0.09)$  and  $\chi_{\text{ndf}}^2 \approx 0.5$  almost coincides with the center of the rectangle from [18]. Finally, the smallest ellipse (thick solid line), entirely enclosed by the previous one, is obtained by unifying the intersections with the  $(a_2, a_4)$  plane of all ellipsoids generated by the variation around the central value of  $\delta^2 = 0.19 \text{ GeV}^2$ . Right panel (‘entire range’): Including into the statistical analysis the high- $Q^2$  tail of the *BABAR* data modifies this picture completely. Now the composed error ellipse resulting from the 2-D analysis (solid blue line) moves out of the region of the negative values of  $a_4$ —characteristic of the BMS models [18]—entering the positive domain. This entails a significantly worse value  $\chi_{\text{ndf}}^2 \approx 2$ , relative to the value  $\chi_{\text{ndf}}^2 \approx 0.5$  for the ‘CLEO-regime’ data set. On the other hand, the unified  $1\sigma$  error ellipse of the 3-D projections on the  $(a_2, a_4)$  plane (larger dashed red ellipse) keeps its position fixed still enclosing the major part of the  $a_2, a_4$  values obtained from nonlocal QCD sum rules (shaded rectangle in green color). Confronting these results with lattice estimates reveals that the 3-D projected error ellipse lies almost entirely within the boundaries from [15] (dashed vertical lines), even intersecting for the larger values of  $a_2$  with the narrower interval determined in [16] (dashed-dotted vertical lines). In contrast to the left panel, the ellipse of the 2-D analysis for the entire set of data only poorly complies with the small  $a_2$  window of [16], while partly overlapping with the low end of the  $a_2$  range determined in [15]. For comparison, some characteristic pion DAs are also shown in Fig. 2: asymptotic DA ( $\blacklozenge$ ); Chernyak-Zhitnitsky (CZ) model [20] ( $\blacksquare$ ); projection of Model III from [13] ( $\blacktriangle$ ).

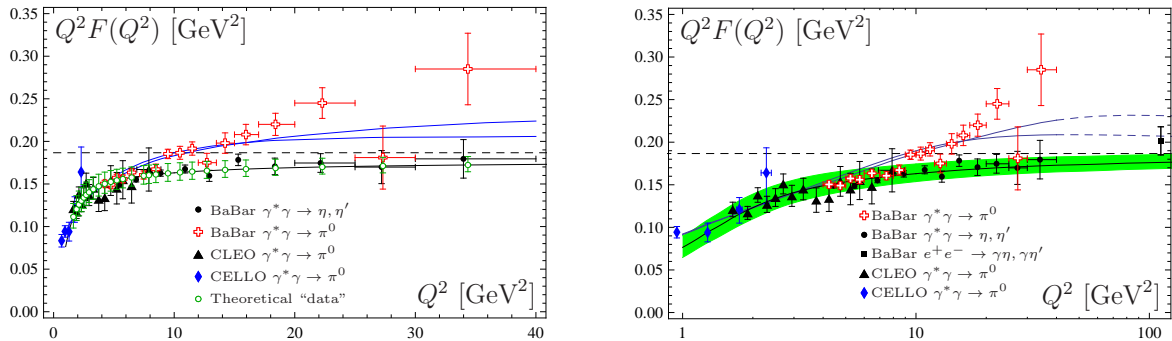


**Fig. 3** (color online).  $Q^2 F^{\gamma^* \gamma \pi^0}(Q^2)$  as a function of  $Q^2$ . Left panel shows “benchmark theoretical data” (open circles) that include systematic uncertainties from different sources, explained in the text, in comparison with real experimental data [1; 2; 4; 6]. Right panel serves to show the large  $Q^2$  form-factor behavior using a logarithmic plot. The shaded (green) strip contains the results for the BMS bunch of  $\pi$  DAs, with the BMS model [18] being represented by a solid line. Also shown are the predictions of Agaev *et al.* [13] for their models I and III, extrapolated in terms of dashed (blue) lines to the remote timelike point  $112 \text{ GeV}^2$  from [21].

Figure 3 shows the calculated pion-photon transition form factor [5] in comparison with various sets of data, specified in the caption. The graphics in the left panel displays the theoretical results in the form of “data” at the same momentum-transfer values as the experimental data and with theoretical uncertainties included as error bars—see Table I in the first work of Ref. [5] for the numerics. The right panel serves to effect the large- $Q^2$  behavior of the scaled form factor—therefore, a logarithmic scale. The shaded green strip embodies the predictions obtained in [5], as described above. One observes: (i) The shaded strip fits the CELLO, CLEO and the ‘CLEO regime’ set of the *BABAR* data very precisely (overall  $\chi^2 < 1$ ). (ii) The prediction approaches asymptotically the limit  $\sqrt{2}f_\pi$  from below and agrees very well with the *BABAR* data for the  $\gamma^* \gamma \eta(\eta')$  transition form factor, being in conflict with the steep rise of the *BABAR* data for  $Q^2 F^{\gamma^* \gamma \pi^0}(Q^2)$  above  $9 \text{ GeV}^2$ . (iii) The LCSR predictions of [13] (single solid blue lines) are not really reproducing the behavior of the *BABAR* data, despite the opposite claims by the authors and the use of pion DAs with a high number of harmonics. In fact, the reinforcement of the form factor can only be achieved by an enhancement of the endpoint region  $x = 0, 1$  of the pion DA, with the best agreement being provided by the flattop DA which includes all  $x$  values in an equal amount, inevitably entailing a worse fit to the data in the ‘CLEO regime’ and below (see [5] for details).

## 4 Conclusions

To conclude, we cannot *predict* the rise of the scaled pion-photon transition form factor, observed by the *BABAR* Collaboration, using the standard scheme of QCD. Nor can we *explain* it in hindsight within the same context—despite opposite claims in [13] and elsewhere [22]. Therefore, the *BABAR* data are unpredictable in QCD, but they are not unexplainable—in particular contexts which, however, are contingent on assumptions that can hardly be accommodated within the standard scheme of QCD. Moreover, there is a dichotomy of the pseudoscalar meson sector into two very disparate groups, one obeying the QCD asymptotics, the other not, depending on the particular shape of the pion DA. Indeed, for BMS-like models (double-humped and endpoint-suppressed) [18], the predictions completely agree with the CELLO [1] and *all* data in the ‘CLEO region’ [2; 4] for the pion-photon transition form factor, as well as with the *BABAR* data [6] for the  $\eta(\eta')$ -photon transition form factor, while being in strong disagreement with the *BABAR* data [4] for the  $\pi^0$ -photon form factor above  $9 \text{ GeV}^2$ . On the other hand, using a flatlike DA [23; 24; 25] (which describes an unrealistic pointlike pion) reproduces the  $\gamma^* \gamma \pi^0$  *BABAR* data but fails to comply with those on the  $\eta(\eta')$ -photon transition leading to predictions above the experimental data [5] (see also [26; 27; 28]). These findings indicate a possible strong violation of the isospin symmetry in the pseudoscalar meson sector ( $\pi^0$  and  $\eta_8$ ) that has not been observed in other measurements so far. Therefore, the reproducibility of the *BABAR* results for the pion-photon transition form factor by other experiments (e.g., by Belle) is of paramount importance.

**Acknowledgements** I am thankful to A.P. Bakulev, S.V. Mikhailov, and A.V. Pimikov for a fruitful collaboration within the Heisenberg-Landau Program (Grant 2011), and to the DAAD for a travel grant.

## References

1. Behrend, H.J. *et al.* (CELLO Collaboration): A measurement of the  $\pi^0$ ,  $\eta$  and  $\eta'$  electromagnetic form-factors. *Z. Phys. C* 49, 401 (1991)
2. Gronberg, J. *et al.* (CLEO Collaboration): Measurements of the meson-photon transition form factors of light pseudoscalar mesons at large momentum transfer. *Phys. Rev. D* 57, 33 (1998)
3. Lepage, G.P., Brodsky, S.J.: Exclusive processes in perturbative quantum chromodynamics. *Phys. Rev. D* 22, 2157 (1980)
4. Aubert, B. *et al.* (BABAR Collaboration): Measurement of the  $\gamma\gamma^* \rightarrow \pi^0$  transition form factor. *Phys. Rev. D* 80, 052002 (2009)
5. Bakulev, A.P., Mikhailov, S.V., Pimikov, A.V., Stefanis, N.G.: Pion-photon transition—the new QCD frontier. *Phys. Rev. D* 84, 034014 (2011); Pion-photon transition form factor using light-cone sum rules: theoretical results, expectations, and a global-data fit. arXiv:11084344 [hep-ph]
6. Sanchez, P. del Amo *et al.* (BABAR Collaboration): Measurement of the  $\gamma\gamma^* \rightarrow \eta$  and  $\gamma\gamma^* \rightarrow \eta'$  transition form factors. arXiv:1101.1142 [hep-ex]
7. Feldmann, T., Kroll, P., Stech, B.: Mixing and decay constants of pseudoscalar mesons. *Phys. Rev. D* 58, 114006 (1998)
8. Khodjamirian, A.: Form factors of  $\gamma^*\rho \rightarrow \pi$  and  $\gamma^*\gamma \rightarrow \pi^0$  transitions and light-cone sum rules. *Eur. Phys. J. C* 6, 477 (1999)
9. Balitsky, I.I., Braun, V.M., Kolesnichenko, A.V.: Radiative Decay  $\sigma^+ \rightarrow p\gamma$  in Quantum Chromodynamics. *Nucl. Phys. B* 312, 509 (1989)
10. Schmedding, A., Yakovlev O.: Perturbative effects in the form factor  $\gamma\gamma^* \rightarrow \pi^0$  and extraction of the pion wave function from CLEO data. *Phys. Rev. D* 62, 116002 (2000)
11. Bakulev, A.P., Mikhailov, S.V., Stefanis, N.G.: Unbiased analysis of CLEO data beyond LO and pion distribution amplitude. *Phys. Rev. D* 67, 074012 (2002); CLEO and E791 data: A smoking gun for the pion distribution amplitude? *Phys. Lett. B* 578, 91 (2004); Tagging the pion quark structure in QCD. *Phys. Rev. D* 73, 056002 (2005)
12. Mikhailov, S.V., Stefanis, N.G.: Transition form factors of the pion in light-cone QCD sum rules with next-to-next-to-leading order contributions. *Nucl. Phys. B* 821, 291 (2009); Two-loop contribution to the pion transition form factor vs. experimental data. *Nucl. Phys. B (Proc. Suppl.)* 198, 199 (2010); Pion transition form factor at the two-loop level vis-à-vis experimental data. *Mod. Phys. Lett. A* 24, 2858 (2009)
13. Agaev, S.S. *et al.* Light cone sum rules for the  $\pi^0\gamma^*\gamma$  form factor revisited. *Phys. Rev. D* 83, 054020 (2011)
14. Efremov, A.V., Radyushkin, A.V.: Asymptotical behavior of pion electromagnetic form factor in QCD. *Theor. Math. Phys.* 42, 97 (1980)
15. Braun, V.M. *et al.*: Moments of pseudoscalar meson distribution amplitudes from the lattice. *Phys. Rev. D* 74, 074501 (2006)
16. Arthur, R. *et al.*: Lattice results for low moments of light meson distribution amplitudes. *Phys. Rev. D* 83, 074505 (2011)
17. Melić, B., Müller, D., Passek-Kumerički, K.: Next-to-next-to-leading prediction for the photon-to-pion transition form factor. *Phys. Rev. D* 68, 014013 (2003)
18. Bakulev, A.P., Mikhailov, S.V., Stefanis, N.G.: QCD-based pion distribution amplitudes confronting experimental data *Phys. Lett. B* 508, 279 (2001); Erratum: *ibid.* B 590, 309 (2006)
19. Stefanis, N.G., Schroers, W., Kim, H.-C.: Pion form factors with improved infrared factorization. *Phys. Lett. B* 449, 299 (1999); Analytic coupling and Sudakov effects in exclusive processes: Pion and  $\gamma^*\gamma \rightarrow \pi^0$  form factors. *Eur. Phys. J. C* 18, 137 (2000)
20. Chernyak, V.L., Zhitnitsky, A.R.: Asymptotic behavior of exclusive processes in QCD. *Phys. Rept.* 112, 173 (1984)
21. Aubert, B. *et al.* (BABAR Collaboration): Measurement of the  $\eta$  and  $\eta'$  transition form factors at  $q^2 = 112 \text{ GeV}^2$ . *Phys. Rev. D* 74, 012002 (2006)
22. Kroll, P.: The form factors for the photon to pseudoscalar meson transitions – an update. *Eur. Phys. J. C* 71, 1623 (2011)
23. Radyushkin, A.V.: Shape of pion distribution amplitude. *Phys. Rev. D* 80, 094009 (2009)
24. Polyakov, M.V.: On the pion distribution amplitude shape. *JETP Lett.* 90, 228 (2009)
25. Mikhailov, S.V., Pimikov, A.V., Stefanis, N.G.: Endpoint behavior of the pion distribution amplitude in QCD sum rules with nonlocal condensates. *Phys. Rev. D* 82, 054020 (2010)
26. Brodsky, S.J., Cao, F.-G., de Teramond, G.F.: Evolved QCD predictions for the meson-photon transition form factors. *Phys. Rev. D* 84, 033001 (2011); Meson transition form factors in light-front holographic QCD. arXiv:1105.3999 [hep-ph]
27. Roberts, H.L.L. *et al.*: Abelian anomaly and neutral pion production. *Phys. Rev. C* 82, 065202 (2010)
28. Wu, X.-G., Huang, T.: Constraints on the Light Pseudoscalar Meson Distribution Amplitudes from Their Meson-Photon Transition Form Factors. arXiv:1106.4365 [hep-ph]